Shap. Mem. Superelasticity (2016) 2:95–103
DOI 10.1007/s40830-016-0054-3

# Ultra-Low Fatigue Quaternary TiNi-Based Films for Elastocaloric Cooling

**C. Chluba[1] · H. Ossmer[2] · C. Zamponi[1] · M. Kohl[2] · E. Quandt[1]**

Published online: 26 February 2016


**Abstract** Elastocaloric applications require superelastic shape memory materials which show high fatigue resistance, adjustable transformation temperatures, short heat transfer times, and large elastocaloric effect sizes. Ti-rich TiNiCu films are known for their high functional and structural stability of several million cycles without any degradation, accompanied by a small hysteresis caused by the good crystallographic compatibility of austenite and martensite phase. Still, for the application of TiNiCu as an elastocaloric cooling agent, transformation temperature adjustment is necessary. Quaternary Co and Fe alloying is found to reduce the transformation temperature by 42 and 22 K at.%$^{-1}$, respectively, while maintaining high transformation enthalpies of 7.9 J g$^{-1}$ for $Ti_{54.7}Ni_{30.7}Cu_{12.3}Co_{2.3}$ films. Furthermore, this specific alloy shows a 25 % larger coefficient of performance compared to binary TiNi films. Combined with the high fatigue resistance, the small transformation strain of 1.6 %, and the operational temperature range of ~50 K, this material is a very attractive candidate for elastocaloric cooling applications.

✉ E. Quandt
eq@tf.uni-kiel.de

C. Chluba
crc@tf.uni-kiel.de

[1] Chair for Inorganic Functional Materials, Faculty of Engineering, Institute for Materials Science, University of Kiel, Kaiserstr. 2, 24143 Kiel, Germany

[2] Institute of Microstructure Technology, Karlsruhe Institute of Technology, Hermann-von-Helmholtz-Platz 1, 76344 Eggenstein-Leopoldshafen, Germany

**Keywords** Superelasticity · Enthalpy of transformation · Transformation strain · Transformation temperature · Elastocaloric effect · Thin films

## Introduction

Ferroic cooling is an emerging field with the aim to develop new cooling agents, characterized by a solid state phase transformation instead of a liquid–vapor transition in conventional cooling devices [1]. This technology has the advantage of environmental compatibility due to the absence of climate damaging gases and a higher theoretical limit of efficiency compared to vapor compression cooling cycles [2]. Depending on the caloric effect i.e., magnetocaloric, electrocaloric, or elastocaloric effect, the transformation can be driven by magnetic, electric, or mechanical stress fields, respectively [3].

For elastocaloric cooling, especially TiNi-based [2, 4–7] and Cu-based [8–10] shape memory alloys (SMAs) have been investigated, which are characterized by a stress or temperature-induced reversible austenite–martensite phase transition. Several requirements have to be fulfilled by this type of material for the use as an elastocaloric cooling agent. First, the functional and structural stability of this material has to be high because it has to withstand several million cycles of stress-induced transformation during the lifetime of a cooling device [2]. Also the adiabatic temperature change during the transformation and the associated transformation enthalpy has to be sufficiently high [10]. Another requirement is a small superelastic hysteresis since it is directly proportional to the dissipated work. These quantities determine the efficiency of the material expressed by the coefficient of performance (COP) which relates the transferred heat of a cooling cycle $Q$ to the

performed work $W$, COP $= Q/W$ [3]. Aim of this work is to investigate only the intrinsic material COP. Major sources of losses in an actual device like parasitic heat flow are not taken into account. Several research groups are working on prototypes based on bulk materials to evaluate not only the intrinsic material COP, but also the whole cooling process efficiencies [11–13].

Instead of conventional bulk technology, the samples investigated within this work are prepared by sputter deposition. Thin film technology allows the production of small structures enabling high cooling power caused by short heat transfer times and small actuator sizes due to low transformation forces. These properties promise the fabrication of miniaturized cooling devices which are demanded e.g., for cooling of mobile microelectronic or lab-on-a-chip systems [14].

Among the NiTi-based materials Ti-rich TiNiCu-based thin films are of special interest due to a smaller hysteresis compared to binary NiTi [15] along with a superior mechanical stability of more than $10^7$ full transformation cycles [16] and good microstructural transformation reversibility [17]. This high durability is necessary because high cycle frequencies of up to 10 Hz are realistic operational conditions for film elastocaloric cooling devices resulting in millions of transformation cycles during the lifetime of the device. Besides the high stability, TiNiCu has the advantage of a low transformation stress hysteresis [18] due to the good compatibility of austenite and martensite phases [19, 20]. This property promises high COPs for this class of material [5] and will be also investigated within the scope of this paper.

Another limiting factor for the application of SMAs as cooling agents is the transformation temperature which determines the operational temperature range of the device. Elastocaloric cooling exploits the temperature decrease of the SMA material caused by the superelastic stress-induced martensite → austenite reverse transformation, thus, the minimum cooling temperature is limited by the austenite finish temperature $A_f$. For real cooling applications, working temperatures higher than $A_f + \Delta T$ have to be used to ensure a fast reverse transformation. Preliminary investigations of Ti-rich TiNiCu films show high cyclic stability of the elastocaloric effect size in TiNiCu films compared to NiTi films [4], nevertheless the minimum cooling temperature of this material is above RT due to the high $A_f$ temperature of ~70 °C. To overcome this problem, quaternary alloying with Co and Fe is investigated which has been reported to decrease the transformation temperature in bulk NiTi alloys [15, 22]. Suitable fatigue resistance for elastocaloric applications of quaternary Ti-rich TiNiCuCo compositions was already shown [16] but the investigation of the related elastocaloric performance is barely explored [17]. Aim of this paper is to close this gap and to examine the influence of Co and Fe addition with regard to the transformation temperature and the elastocaloric parameters.

## Experimental

Amorphous films with a composition of $(Ti_{55}Ni_{33}Cu_{12})_{100-x}Co_x$ with $x = (1.3, 2.4, 3.6, 5.3)$ at.% and $(Ti_{55}Ni_{33}Cu_{12})_{100-x}Fe_x$ with $x = (1.3, 2.4, 3.6, 5.3)$ at.% measured by EDX (FEI Helios Nanolab 600) have been prepared by multilayer sputtering of 35 nm TiNiCu and 0.5–1 nm Co/Fe using an Von Ardenne CS 730S with a 4″ $Ti_{56}Ni_{29}Cu_{15}$ at.% alloy target manufactured by TMI and a single element 8″ Co and Fe targets. Different sputter parameters (DC, 300 W, 20 sccm, $1.6 \times 10^{-3}$ mbar Ar) for TiNiCu and (DC, 20 W, 20 sccm, $1.6 \times 10^{-3}$ mbar Ar) for Co and (RF, 200 W, 20 sccm, $1.6 \times 10^{-3}$ mbar Ar) for Fe are used to deposit 250 and 500 alternating layers, resulting in a total film thickness of 9 µm and 18 µm, respectively. The SMA films are deposited on a sacrificial Cu layer to obtain freestanding films according to a previously published process [21]. Subsequently the amorphous multilayered films are homogenized and crystallized at 700 °C for 15 min by applying rapid thermal annealing (RTA). Additionally, 18 µm $Ti_{55}Ni_{33}Cu_{12}$ single-layer films are annealed at 600 °C for 15 min and also at 500 °C for 15 min.

To investigate the diffusion of Co in TiNiCu, a FIB cross section, perpendicular to the multilayer stack is prepared (FEI Helios Nanolab 600) and an element mapping is performed by STEM/EDX using a JEOL JM2100 at 200 keV.

Differential scanning calorimetry (DSC) measurements with a Perkin Elmer DSC 1 are conducted with 3 mg sample weight and a heating rate of 10 K $min^{-1}$. Transformation temperatures have been determined with the tangent method, the latent heats $Q_{A-M}$ and $Q_{M-A}$ by integration of the heat flow peaks using a linear baseline. Due to the low investigated sample weight caused by the small sample thickness, an enthalpy error of $Q = 0.5$ J $g^{-1}$ is assumed.

Tensile tests, utilizing a Zwick Roell Z.05 with an attached heating and cooling chamber, are performed isothermally at a low strain rate of 0.01 $min^{-1}$ to avoid self-heating of the sample during the measurement. Different temperatures above $A_f$ for the individual samples are used for the tensile test. The upper yielding point was chosen as the end of the transformation plateau. Tests with higher strain rates of 0.008–1.1 $s^{-1}$ are performed to measure the temperature change of the material close to adiabatic conditions. For the IR tests, the samples are coated with graphite spray (Tetenal camera varnish), with

an IR emission factor of 0.96. IR thermograms, recorded by an IR camera (InfraTec PIR 180), are averaged over an emission corrected area of 10 px × 10 px (700 µm × 700 µm) and used to calculate the temperature change.

## Results and Discussion

### DSC Measurements

The influence of the heat treatment and the addition of Fe and Co on the thermal transformation properties of TiNiCu is investigated by DSC (differential scanning calorimetry) measurements. The Fe and Co content is adjusted using a multilayer sputtering approach by depositing layers of 35 nm TiNiCu, alternating with <1 nm thin layers of Fe or Co. All DSC measurements reveal single-peak forward and reverse transformations, indicating a homogeneous Fe and Co distribution within the annealed multilayer structure. The homogeneous mixture is also verified by STEM/EDX mappings (not shown).

Austenite finish temperatures $A_f$ and martensite finish temperatures $M_f$ are determined using the tangent method. For the TiNiCuX compositions with $X$ = (Fe, Co), a linear transformation temperature shift to lower temperatures is observed by 42 and 22 K at.%$^{-1}$ for the addition of Fe and Co, respectively, as shown in Table 1 and Fig. 1a. This transformation temperature reduction has also been reported for $Ti_{50}Ni_{(45-x)}Cu_5Co_x$ bulk samples with a similar temperature shift of 17 K at.%$^{-1}$ for Co addition [22].

Annealing of ternary TiNiCu at lower temperatures of 600 °C for 15 min and also at 500 °C for 15 min is investigated as an alternative to the use of quaternary elements for the adjustment of the transformation temperatures. With lower annealing temperature, a decrease of $A_f$ is observed, shown in Fig. 1b, a relation which has been already reported for Ti-rich TiNiCu films and is contributed to the formation of Guinier–Preston zones at lower annealing temperatures [23].

Equation $\Delta H = (Q_{A-M} + Q_{M-A})/2$ was used to calculate the transformation enthalpy, taking into account the additionally generated heat due to irreversible processes during the transformation [24]. Major parameters for elastocalorics, $A_f$ and $\Delta H$, are shown in Fig. 1b, showing that the decrease of transformation temperature also leads to a decrease of the transformation enthalpy with a similar slope for both, Fe and Co. Figure 1b also reveals that using quaternary systems is the better option to adjust the transformation temperature for room temperature use, since for a required $A_f$ temperature of approximately 10 °C, the TiNiCuCo and TiNiCuFe show a $\Delta H$ of 7.9 and 7.5 J g$^{-1}$, while the TiNiCu sample annealed at 500 °C only exhibits a $\Delta H$ of 4.8 J g$^{-1}$.

### Tensile Tests

To investigate the influence of the alloying on the stress–strain behavior, TiNiCuFe samples containing different Fe contents are tested at temperatures of 10 K above their individual $A_f$ temperatures, Fig. 2a. The general transformation behavior characteristics like transformation strain, stress plateau, and hysteresis are not influenced by the alloying. Tensile tests at sequential temperatures above $A_f$ are used to measure the Clausius–Clapeyron coefficients ($d\sigma_{trans}/dT$) which describe the change of transformation stress $\sigma_{trans}$ with temperature (stress–strain curves of $Ti_{54.7}Ni_{30.7}Cu_{12.3}Co_{2.3}$ at different test temperatures are shown, representatively, Fig. 2b). The Clausius–Clapeyron coefficient is proportional to the operational temperature range of the elastocaloric material with $A_f$ as lower limit and the approximation $A_f + \sigma_{max}/(d\sigma_{trans}/dT)$ as upper limit ($\sigma_{max}$ is the maximum stress limit for reversible deformations). Measurements of different compositions reveal that the Clausius–Clapeyron coefficient is almost not influenced by the addition of Co and Fe, Fig. 2c.

**Table 1** DSC measurement of $(Ti_{55}Ni_{33}Cu_{12})_{(100-x)}Fe_x$ and $(Ti_{55}Ni_{33}Cu_{12})_{(100-x)}Co_x$ annealed at 700 °C for 15 min of austenite finish temperature $A_f$, martensite finish temperature $M_f$, latent heats of martensite $Q_{A-M}$ and austenite $Q_{M-A}$ transformation, transformation peak temperatures, and the calculated hysteresis $\Delta T$ (peak–peak) and transformation enthalpy $\Delta H$

| at.% | $A_f$ (°C) | $Q_{M-A}$ (J g$^{-1}$) | $M_f$ (°C) | $Q_{A-M}$ (J g$^{-1}$) | Peak$_{M-A}$ (°C) | Peak$_{A-M}$ (°C) | $\Delta T$ (K) | $\Delta H$ (J g$^{-1}$) |
|---|---|---|---|---|---|---|---|---|
| Fe 0.7 | 35 | 8.1 | 15 | −9.5 | 33.9 | 18 | 15.9 | 8.8 |
| Fe 1.3 | 6 | 7 | −14 | −7.9 | 4.6 | −11.6 | 16.2 | 7.5 |
| Fe 1.6 | −6 | 5 | −26 | −6.7 | −8.1 | −22.8 | 14.7 | 5.9 |
| Co 1.3 | 40 | 8.8 | 20 | −9.3 | 37 | 23 | 14 | 9 |
| Co 2.4 | 8 | 6.8 | −12 | −9.1 | 5.7 | −11 | 16.7 | 7.9 |
| Co 3.6 | −13 | 6.2 | −32 | −6 | −15 | −30 | 15 | 6.1 |
| Co 5.3 | −50 | 2.9 | −68 | −2.6 | −52.8 | −65 | 12.2 | 2.8 |

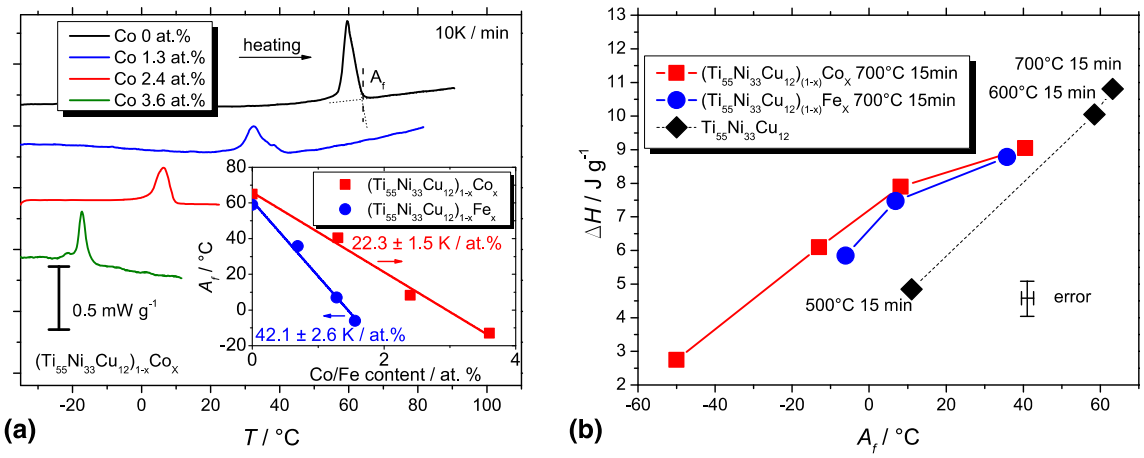


**Fig. 1** **a** DSC measurements of $(Ti_{55}Ni_{33}Cu_{12})_{(100-x)}Co_x$ with different Co contents (large). Change of the austenite finish temperature $A_f$ in dependence of Co and Fe content (*inset*). **b** Relation of transformation enthalpy $\Delta H$ versus $A_f$ for quaternary compositions with different Co and Fe contents annealed at 700 °C 15 min and additionally for ternary $Ti_{55}Ni_{33}Cu_{12}$ composition annealed at 500, 600, and 700 °C for 15 min

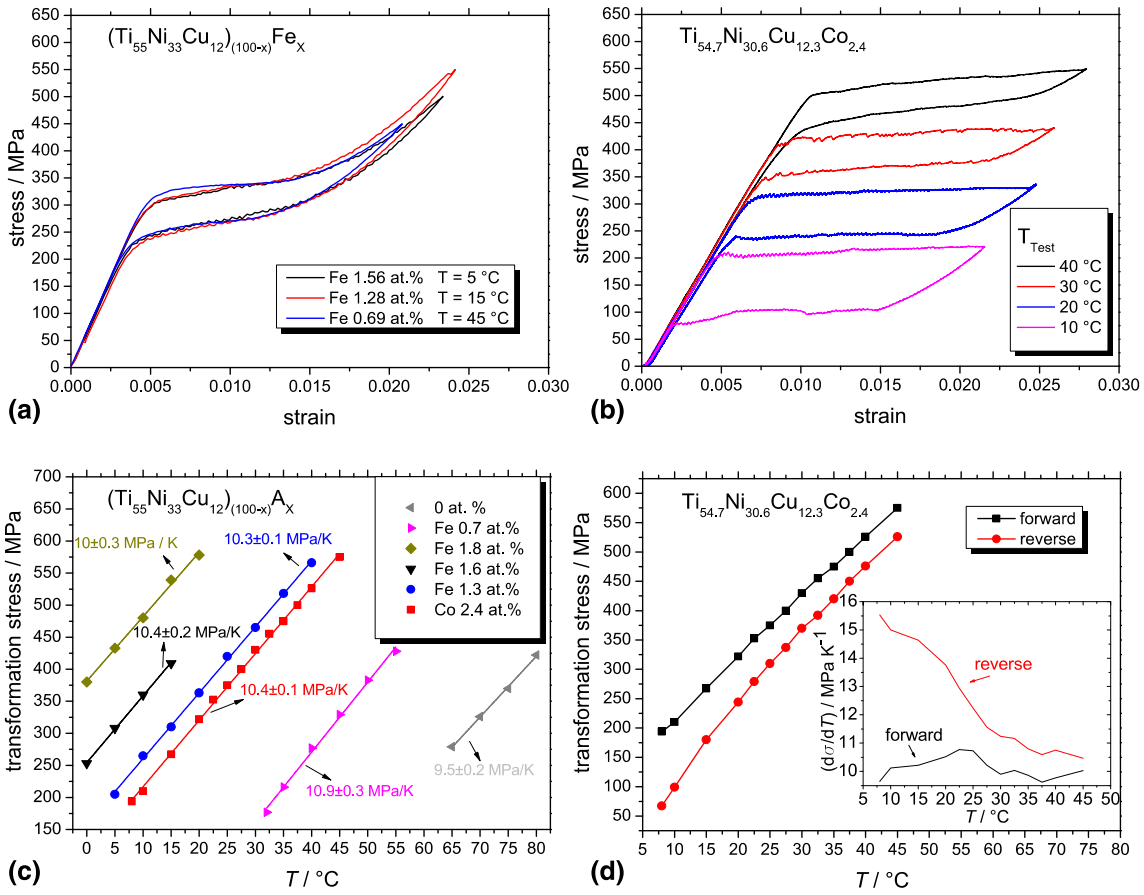


**Fig. 2** **a** Superelastic tensile tests of different TiNiCuFe compositions at a test temperature at 10 K above $A_f$. **b** Tensile tests of $Ti_{54.7}Ni_{30.7}Cu_{12.3}Co_{2.3}$ at different test temperatures (4 of 13 curves are shown representatively). **c** Clausius–Clapeyron forward transformation coefficients for different compositions. Transformation stresses are measured similarly as shown in **b**, by temperature dependent tensile tests. **d** Transformation stresses of $Ti_{54.7}Ni_{30.7}Cu_{12.3}Co_{2.3}$ forward and reverse transformation for different test temperatures. The corresponding slope d$\sigma$/d$T$ known as the Clausius–Clapeyron coefficient is calculated by numerical differentiation (*inset*)

To investigate the Clausius–Clapeyron coefficient of forward and reverse transformation, the transformation stress of $Ti_{54.7}Ni_{30.7}Cu_{12.3}Co_{2.3}$, Fig. 2d, has been differentiated numerically Fig. 2d(inset) [8]. The austenite → martensite transformation shows an almost constant Clausius–Clapeyron coefficient of $10.4 \pm 0.1$ MPa $K^{-1}$ (linear fit) while for the reverse martensite → austenite transformation it is increasing from 10.5 to 15.5 MPa $K^{-1}$ close to the $A_f$ temperature. This effect and the related larger hysteresis close to the $A_f$ temperatures could be observed for all investigated compositions and is also known for binary NiTi alloys [25]. Since the hysteresis is directly proportional to the performed work, the temperature difference of $A_f$ to test temperature has to be taken into account for efficiency estimations.

In combination with the transformation strain $\Delta\varepsilon$ and the specific volume $V_0$, the Clausius–Clapeyron coefficient enables the approximation of the transformation entropy by applying Maxwell equation [8], $\Delta S = V_0(d\sigma_{trans}/dT)\Delta\varepsilon$. The enthalpy change can be calculated by $\Delta H = T_0 \cdot \Delta S$ with $T_0 = (A_f - M_f)/2$. Tensile test parameters of $Ti_{54.7}Ni_{30.7}Cu_{12.3}Co_{2.3}$ at 20 °C are used for the calculation, Fig. 2b/c. With $\Delta\varepsilon = 0.0177$, $(d\sigma_{trans}/dT) = 10.5$ MPa $K^{-1}$ for the forward, $\Delta\varepsilon = 0.0135$, $(d\sigma_{trans}/dT) = 13.5$ MPa $K^{-1}$ for the reverse transformation, and $V_0 = 1.55 \times 10^{-4}$ $m^3$ $kg^{-1}$ the enthalpy results in $\Delta H = 8.5$ J $g^{-1}$ and $\Delta H = 8.2$ J $g^{-1}$, respectively, which is in good agreement with the DSC measurement of 7.9 J $g^{-1}$. As previously reported [25], the measurement also shows that the increase of the Clausius–Clapeyron coefficient close to the transformation temperature is compensated by smaller transformation strains of the martensite → austenite transformation compared to the austenite–martensite transformation yielding similar transformation enthalpies for forward and reverse transformation.

To calculate the evolution of the isothermal entropy change for different test temperatures, the fundamental equation of the entropy approximation used above is considered. Based on the thermodynamic equation derived from Clausius–Clapeyron and Maxwell equation in previous publications [8], isothermal tensile test at different test temperatures can be used to calculate isothermal entropy change according to

$$\Delta S(0 \rightarrow \sigma) = \int_0^{\sigma} \left(\frac{\partial \varepsilon}{\partial T}\right)_{\sigma} d\sigma. \quad (1)$$

For this evaluation, the strain–stress curves of forward austenite → martensite and backward martensite → austenite transformation are interpolated, as shown in Fig. 3a, b, to enable a numerical differentiation with constant stress $\left(\frac{\partial \varepsilon}{\partial T}\right)_{\sigma}$, shown in Fig. 3c, d. Integration boundaries from 0 MPa to the stress at which the transformation is completed are used for the individual temperatures and the integration results are shown in Fig. 3e. Entropy differences of forward and reverse transformation are small and can be considered within the error of this evaluation. The change of entropy with temperature shows a decreasing trend with increasing test temperature.

## COP Measurement by Infrared Thermography

To determine the cooling capabilities of this class of alloys, $Ti_{54.7}Ni_{30.7}Cu_{12.3}Co_{2.3}$ is investigated representatively with respect to the COP which is defined as transported heat $Q$ per performed work $W$, Eq. 2.

$$\mathrm{COP} = \frac{Q(\Delta T, T_{amb})}{W(\Delta T, T_{amb})} \quad (2)$$

For an elastocaloric cooling cycle both quantities, $Q$ and $W$, depend on the heat sink temperature $T_{amb}$ and the temperature difference $\Delta T$ between heat sink and the colder heat source. For the comparison of different elastocaloric materials, in general, only the case $\Delta T = 0$ K is taken into account where the complete latent heat of the reverse transformation can be extracted from the heat source [2, 6]. From the variety of possible elastocaloric cooling cycles, the following four step procedure is used to determine the COP:

(1) Tensile loading at $T_{amb}$ with different strain rates.
(2) Heat flow to environment until $T_{amb}$ is reached again.
(3) Unloading at different strain rates. The negative adiabatic temperature change $\Delta T$ is used to calculate $\Delta H$.
(4) Heat exchange with environment until $T_{amb}$ is reached again.

The work per volume is described by the hysteresis area of the stress–strain curve, measured from step (1) to step (4), because the unused work during the reverse transformation can be theoretically regained by an appropriate device setup. Tensile loading and unloading tests similar to those shown in Fig. 2b, are performed at room temperature with different strain rates and stress–strain curves have been integrated numerically to obtain the performed work of loading and unloading according to $\Delta W = \oint \sigma d\varepsilon$, shown in Fig. 4a [26].

The transferred heat is difficult to measure directly, thus the indirect method by measuring the adiabatic temperature change during the strain-induced transformation is used to calculate the transformation enthalpy. This quantity can also be accessed by DSC measurements, but due to differences in strain and temperature-induced transformations,

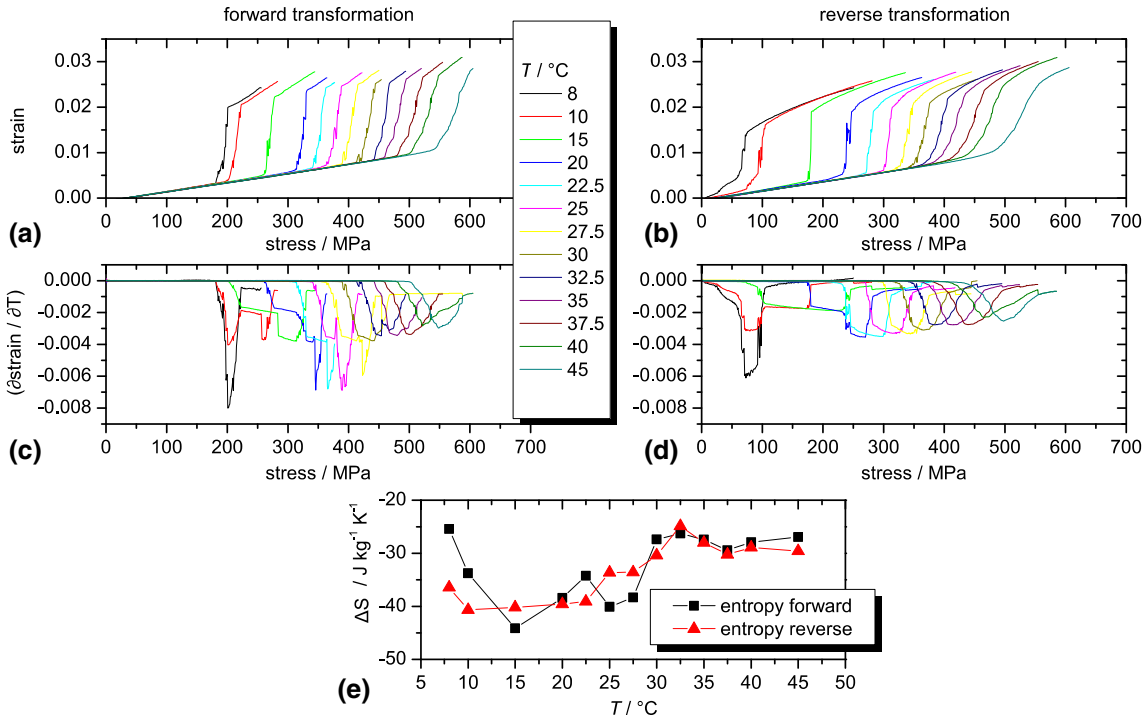


**Fig. 3** Calculation of the superelastic entropy change based on isothermal tensile tests at different ambient temperatures according to $\Delta S(0 \rightarrow \sigma) = \int_0^\sigma \left(\frac{\partial \varepsilon}{\partial T}\right)_\sigma \mathrm{d}\sigma$. **a**, **b** The interpolated superelastic stress–strain curves for the forward austenite → martensite and the reverse martensite → austenite transformation for different temperatures. **c**, **d** The differential $\left(\frac{\partial \varepsilon}{\partial T}\right)_\sigma$ which is used to calculate the entropy change for different test temperatures is shown in **e**. Calculation is performed by numerical integration from zero stress to the stress value of finished transformation (end of $\left(\frac{\partial \varepsilon}{\partial T}\right)_\sigma$ vs. stress peak)

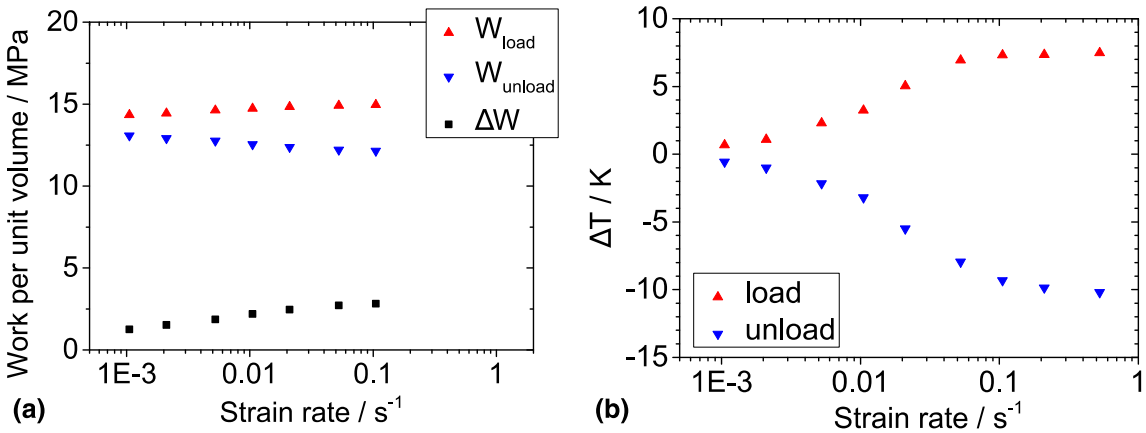


**Fig. 4** **a** Specific work of $Ti_{54.7}Ni_{30.7}Cu_{12.3}Co_{2.3}$ for the stress-induced martensite transformation (loading) and reverse transformation (unloading) as a function of strain rate, respectively. The difference $\Delta W = W_{\mathrm{load}} - W_{\mathrm{unload}}$ represents the work input (dissipated energy) per load–unload cycle. **b** Peak temperature rise during mechanical loading and peak temperature drops during unloading as a function of strain rate. The adiabatic limit is approached for a strain rate of 0.2 $s^{-1}$

the used method yields more accurate results for elastocaloric cooling [27]. Tensile tests at different strain rates have been conducted while temperature changes are measured by IR thermography, shown in Fig. 4b [5]. At certain strain rates of approximately 0.2 $s^{-1}$, constant conditions are obtained, resulting in an adiabatic temperature change of +7.5 K and −10.2 K for loading and unloading, respectively. The adiabatic temperature change is used to calculate the transformation enthalpy of the reverse transformation which equals the maximum transferable heat with $\Delta H = c_p \cdot \Delta T$. The heat capacity $c_p$ is determined by DSC according to ASTM standard, resulting in

0.42 J (g K)$^{-1}$ for the stress-free austenite phase. The transformation enthalpy results in $\Delta H_{M-A} = 4.28$ J g$^{-1}$ for the reverse transformation which corresponds to the heat that can be extracted from the heat source. It has to be pointed out that the higher negative temperature change is not explained yet and needs further investigation. With the corresponding specific work of $W = 2.8$ MPa (0.38 J g$^{-1}$), under adiabatic loading and unloading conditions, a COP of 10 is obtained.

To investigate the effect of the ambient temperature on the elastocaloric parameters, similar measurements at strain rates from 0.00016 to 0.5 s$^{-1}$ are performed in a climate chamber at different test temperatures from 8 to 45 °C, which is considered to be the temperature range of use. 8 °C is the $A_f$ temperature defining the lower limit while 45 °C corresponds to a transformation stress of 600 MPa, which is assumed to be the maximum reversible stress level. Tensile tests at 30 °C are plotted in Fig. 5a for different strain rates. For strain rates higher than 0.2 s$^{-1}$ measurement artifacts occur, caused by the tensile test machine during the mechanical loading. Therefore 0.5 s$^{-1}$ is excluded from the work evaluation.

In this investigation, the measured negative temperature changes $\Delta T$, shown in Fig. 5b, are lower compared to the data obtained at room temperature for the strain rate variation, shown in Fig. 4b, even if the constant $\Delta T$ regime is reached at 0.5 s$^{-1}$, since the thin sample is exposed to a constant airstream of the climate chamber. Nevertheless, the main focus of this investigation is not to obtain absolute values but the evolution of the elastocaloric parameters at different test temperatures. It is found that the adiabatic temperature change is almost constant for the whole temperature range, but with a slight decrease at higher ambient temperatures, Fig. 5b. This behavior is in good agreement with the entropy calculations from the tensile tests and might be caused by the higher transformation stresses at higher temperatures which decreases the fraction of transforming volume. A more inhomogeneous stress-induced transformation with increasing temperature is also indicated by the change from a flat transformation plateau at 20 °C to a larger slope at 40 °C, Fig. 2b.

The evolution of the performed work with test temperature from 15 to 45 °C differs for the investigated strain rates. While for the slow strain rate of 0.00016 s$^{-1}$, the performed work per volume decreases from 2 to 1 MPa due to the reduced hysteresis, this effect is not so dominant for higher strain rates of 0.2 s$^{-1}$ where only a reduction from 4.25 to 3.2 MPa occurs. Tests at 30 °C with different strain rates show a reduction of the performed work form 3.5 MPa for 0.2 s$^{-1}$ to 3.22 MPa for 0.05 s$^{-1}$ accompanied by a reduction of temperature change from 6.7 to 5.5 °C.

The evolution of the COP with operating temperature is calculated for high strain rates using the adiabatic temperature change and the work performed at 0.2 s$^{-1}$. This investigation yields a constant COP of ~5 over the whole operational temperature range. For lower strain rates of 0.1 and 0.05 s$^{-1}$, the smaller temperature change is compensated by smaller required work which results in similar COPs compared to 0.02 s$^{-1}$. For completeness also, the COP calculated with the isothermal work at 0.00016 s$^{-1}$ and the transformation enthalpy is depicted. In this case the amount of transferred heat is assumed to be the same as in the adiabatic case but no temperature gradient is established, thus, no realistic operational cooling efficiencies are described. Nevertheless, this calculation allows a comparison to the Carnot cycle for which the COP approaches infinity instead of 20 in this case. It also enables the comparison to other elastocaloric materials when isothermal tensile tests and DSC measurements are used for the calculation.

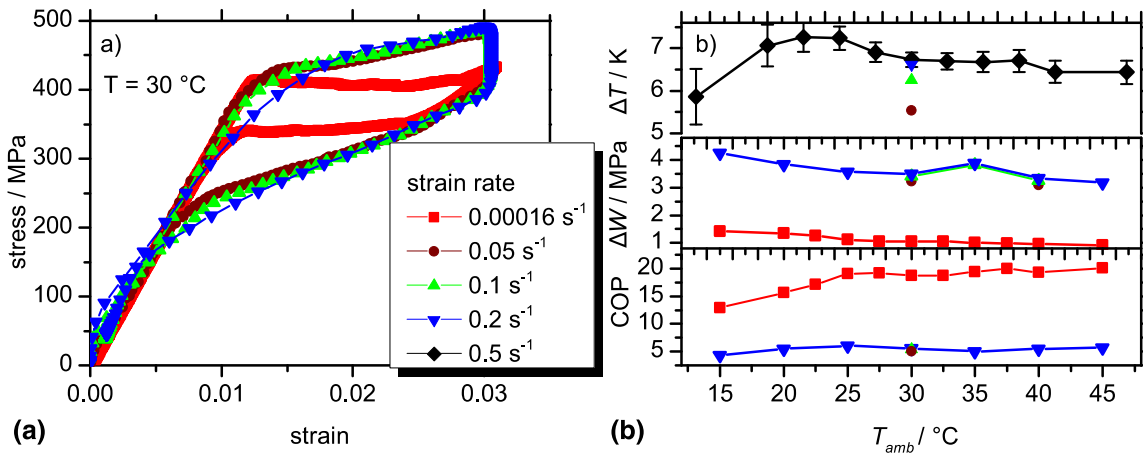


**Fig. 5** **a** Stress–strain curves at 30 °C using strain rates from 0.00016 to 0.2 s$^{-1}$. **b** Temperature change $\Delta T$ during the reverse transformation at fast strain rates, performed work $\Delta W$ obtained by numerical integration at different strain rates and the related COP

## Conclusion

It has been found that the transformation temperature in SMA thin films can be easily adjusted by adding Co or Fe using a multilayer approach. A precise control of the $A_f$ temperature is necessary to adjust the working temperature of a cooling device and is especially important for cascaded cooling processes realized by stacked cooling agents or regenerator systems [12]. These concepts are necessary to obtain suitable cooling intervals $\Delta T$, larger than the intrinsic adiabatic temperature change.

The transformation strain of TiNiCu alloys is with $\sim$1.6 % relatively small compared to binary NiTi ($\sim$4–6 %) or Cu-based ($\sim$6–8 %) alloys [15]. This is an advantage regarding the fatigue behavior, because the microstructure is exposed to less deformation. Also the required actuator stroke decreases correspondingly, giving rise to the use of efficient alternative actuation concepts like piezoelectric transducers. This is of special interest for elastocaloric thin film devices where compact actuation systems are required. Despite the small transformation strain, the adiabatic temperature change of 10 K is comparable to NiTi thin films (16 K) [5] and Cu-based (7 K) [10] alloys, caused by the large Clausius–Clapeyron coefficient of 10 MPa $K^{-1}$ compared to 7 and 1.79 MPa $K^{-1}$, respectively. Disadvantage of the high Clausius–Clapeyron coefficient is the drastic change of the transformation stress plateau with temperature, limiting the operational temperature range to only $\sim$50 K for a stress range up to 600 MPa. This stress level is just an estimation, and the stress-limitation regarding reversibility and fatigue life needs further investigation.

Due to the small transformation strain and small hysteresis of 50–100 MPa for TiNiCu-based SMAs compared to >200 MPa for binary NiTi [4], less work has to be performed, yielding a higher COP of 10 compared to 8, respectively. It is found that the adiabatic temperature change and the COP are almost constant for different test temperatures up to 600 MPa. The evolution of the performed work with test temperature depends on the strain rate. For the isothermal loading case, the work decreases with increasing test temperature due to a smaller hysteresis caused by asymmetric Clausius–Clapeyron coefficients of forward and reverse transformation close to the $A_f$ transformation temperature. In contrast, for adiabatic straining conditions the work remains almost constant throughout the tested temperature range.

In conclusion, this investigation reveals that high fatigue resistant Ti-rich TiNiCu-based alloys exhibit good elastocaloric cooling performance which makes them promising candidates for future elastocaloric cooling applications.

**Acknowledgments** The authors would like to thank the DFG for funding within the Priority Program SPP 1599.

## References

1. Fähler S, Rößler UK, Kastner O et al (2012) Caloric effects in ferroic materials: new concepts for cooling. Adv Eng Mater 14:10–19. doi:10.1002/adem.201100178
2. Cui J, Wu Y, Muehlbauer J et al (2012) Demonstration of high efficiency elastocaloric cooling with large ΔT using NiTi wires. Appl Phys Lett 101:073904. doi:10.1063/1.4746257
3. Moya X, Kar-Narayan S, Mathur ND (2014) Caloric materials near ferroic phase transitions. Nat Mater 13:439–450. doi:10.1038/nmat3951
4. Bechtold C, Chluba C, de Miranda RL, Quandt E (2012) High cyclic stability of the elastocaloric effect in sputtered TiNiCu shape memory films. Appl Phys Lett. doi:10.1063/1.4748307
5. Ossmer H, Lambrecht F, Gültig M et al (2014) Evolution of temperature profiles in TiNi films for elastocaloric cooling. Acta Mater 81:9–20. doi:10.1016/j.actamat.2014.08.006
6. Schmidt M, Ullrich J, Wieczorek A et al (2015) Thermal stabilization of NiTiCuV shape memory alloys: observations during elastocaloric training. Shape Mem Superelasticity 1:132–141. doi:10.1007/s40830-015-0021-4
7. Tušek J, Engelbrecht K, Mikkelsen LP, Pryds N (2015) Elastocaloric effect of Ni-Ti wire for application in a cooling device. J Appl Phys 117:124901. doi:10.1063/1.4913878
8. Bonnot E, Romero R, Mañosa L et al (2008) Elastocaloric effect associated with the martensitic transition in shape-memory alloys. Phys Rev Lett 100:1–4. doi:10.1103/PhysRevLett.100.125901
9. Mañosa L, Planes A, Vives E et al (2009) The use of shape-memory alloys for mechanical refrigeration. Funct Mater Lett 02:73–78. doi:10.1142/S1793604709000594
10. Mañosa L, Jarque-Farnos S, Vives E, Planes A (2013) Large temperature span and giant refrigerant capacity in elastocaloric Cu-Zn-Al shape memory alloys. Appl Phys Lett 103:211904. doi:10.1063/1.4832339
11. Schmidt M, Schütze A, Seelecke S (2015) scientific test setup For investigation of Shape memory alloy based elastocaloric cooling processes. Int J Refrig. doi:10.1016/j.ijrefrig.2015.03.001
12. Tušek J, Engelbrecht K, Millán-Solsona R et al (2015) The elastocaloric effect: a way to cool efficiently. Adv Energy Mater. doi:10.1002/aenm.201500361
13. Cui J (2014) Thermoelastic cooling using nitinol alloy. Present. international conference on martensitic transformations, Bilbao, Spain, July 2014
14. Chow AW (2002) Lab-on-a-chip: opportunities for chemical engineering. AlChE J 48:1590–1595. doi:10.1002/aic.690480802
15. Otsuka K, Ren X (2005) Physical metallurgy of Ti-Ni-based shape memory alloys. Prog Mater Sci 50:511–678. doi:10.1016/j.pmatsci.2004.10.001
16. Chluba C, Ge W, De Miranda RL et al (2015) Ultralow-fatigue shape memory alloy films. Science 348:1004–1007. doi:10.1126/science.1261164
17. Ossmer H, Chluba C, Gueltig M et al (2015) Local evolution of the elastocaloric effect in TiNi-based films. Shape Mem Superelasticity 1:142–152. doi:10.1007/s40830-015-0014-3
18. Nam TH, Saburi T, Shimizu K (1990) Cu-content dependence of shape memory characteristics in Ti-Ni-Cu alloys.pdf. Mater Trans 31:959–967
19. Cui J, Chu YS, Famodu OO et al (2006) Combinatorial search of thermoelastic shape-memory alloys with extremely small hysteresis width. Nat Mater 5:286–290. doi:10.1038/nmat1593

20. Chen X, Srivastava V, Dabade V, James RD (2013) Study of the cofactor conditions: conditions of supercompatibility between phases. J Mech Phys Solids 61:2566–2587. doi:10.1016/j.jmps.2013.08.004
21. Lima de Miranda R, Zamponi C, Quandt E (2012) Micropatterned freestanding superelastic TiNi films. Adv Eng Mater. doi:10.1002/adem.201200197
22. Frenzel J, Wieczorek A, Opahle I et al (2015) On the effect of alloy composition on martensite start temperatures and latent heats in Ni–Ti-based shape memory alloys. Acta Mater 90:213–231. doi:10.1016/j.actamat.2015.02.029
23. Ishida A, Sato M, Gao Z (2014) Effects of Ti content on microstructure and shape memory behavior of Tix-Ni(84.5 − x)Cu15.5 (x = 44.6–55.4) thin films. Acta Mater 69:292–300. doi:10.1016/j.actamat.2014.02.006
24. Salzbrenner RJ, Cohen M (1979) On the thermodynamics of thermoelastic martensitic transformations. Acta Metall 27:739–748. doi:10.1016/0001-6160(79)90107-X
25. Liu Y, Yang H (2007) Strain dependence of the Clausius–Clapeyron relation for thermoelastic martensitic transformations in NiTi. Smart Mater Struct 16:S22–S27. doi:10.1088/0964-1726/16/1/S03
26. Schmidt M, Schütze A, Seelecke S (2013) Cooling efficiencies of a NiTi-based cooling process. In: Proceedings of the ASME 2013 conference on smart materials
27. Ossmer H, Chluba C, Krevet B et al (2013) Elastocaloric cooling using shape memory alloy films. J Phys Conf Ser 476:012138. doi:10.1088/1742-6596/476/1/012138